Appl Phys A (2013) 112:517–523
DOI 10.1007/s00339-013-7782-4

Applied Physics A
Materials Science & Processing

Silicon and porous silicon mid-infrared photonic crystals

Zhiya Dang · Agnieszka Banas · Sara Azimi · Jiao Song · Mark Breese · Yong Yao · Shuvan Prashant Turaga · Gonzalo Recio-Sánchez · Andrew Bettiol · Jeroen Van Kan

Received: 26 April 2013 / Accepted: 16 May 2013 / Published online: 31 May 2013
© Springer-Verlag Berlin Heidelberg 2013

Abstract A 3D silicon micromachining method based on proton beam writing combined with electrochemical anodization of p-type silicon enables fabrication of mid-infrared photonic crystals made of silicon and porous silicon. Here, example structures of silicon 1D and 2D photonic crystals are demonstrated. Progress and problems of fabricating 3D photonic crystals made of silicon are discussed. The strategy of fabricating photonic crystals purely made of porous silicon, and the characterization method of all these mid-infrared structures, are discussed. Due to the flexibility of this fabrication method, photonic devices and integrated photonic circuits may be built on a single chip, for which two 2D silicon photonic crystals with one on top of the other are demonstrated.

1 Introduction

Photonic crystals are dielectric structures with a periodically modulated refractive index, which interact with photons of a comparable wavelength in the equivalent electromagnetic range [1, 2]. Photonic crystals are the building blocks for photonic circuits, incorporating line defects as waveguides, or point defects as cavities and their coupled elements [3]. Photonic circuits are a very useful platform which has promising applications in optofluidics, aiming at manipulating fluids and light at the microscale and exploiting their interaction to create highly versatile systems [4], biological sensing, optoelectronics, etc. Silicon has a high dielectric constant, which enables a high index contrast with air and easier realization of a complete photonic band gap for silicon-based photonic crystals. A silicon photonic crystal is also highly compatible and can be integrated with the IC industry.

Silicon is a semiconductor, which enables the potential application of silicon-based photonic crystals in fabricating active devices, where photons act as switches for particular applications. Porous silicon is produced from electrochemical anodization of silicon, which has large surface area, enabling its advantage in applications in sensing, etc. Besides, porous silicon is biodegradable [5], so porous silicon photonic crystals have potential in biological and medical applications. The refractive index is determined by the porosity of the porous silicon. Porous silicon can be infiltrated with a variety of media, which enables the tunability of photonic band gaps [6]. Therefore, silicon and porous silicon based photonic crystals have advantages that enable their corresponding applications in biological science, medicine, optoelectronics, and optofluidics.

Until now, most silicon and porous silicon based photonic crystals that have been studied are in the visible or near-infrared range, which have sizes of tens to hundreds of nanometers. The top-down approach mainly used for fabrication is electron beam writing of a photoresist coated on a device layer of a silicon-on-insulator wafer, and a further pattern transfer to a device silicon layer by reactive ion etching [7]. The optics for this wavelength range is relatively

Z. Dang (✉) · S. Azimi · J. Song · M. Breese · Y. Yao · S.P. Turaga · A. Bettiol · J.V. Kan
Centre for Ion Beam Applications (CIBA), Department of Physics, National University of Singapore, Singapore 117542, Singapore
e-mail: rongmeijiaoyin@gmail.com

A. Banas · M. Breese
Singapore Synchrotron Light Source (SSLS), National University of Singapore, 5 Research Link, Singapore 117603, Singapore

G. Recio-Sánchez
Departamento de Física Aplicada, Universidad Autónoma de Madrid, 28049 Cantoblanco, Madrid, Spain

mature, allowing photonic crystals to be easily characterized. Very few studies of photonic crystals have been carried out in the mid-infrared range, although the period required is much larger. The main issue is the lack of optical components for the mid-infrared range. Mid-infrared light is widely used in industrial, scientific, and medical applications. Mid-infrared 3D inverse woodpile structures have previously been fabricated by direct laser writing to create a polymer template, and transferred to silicon using chemical vapor deposition [8]. Mid-infrared 2D photonic crystals of a hexagonal lattice with a high aspect ratio have been fabricated by macroporous silicon formation in n-type silicon [9].

In electrochemical anodization of p-type silicon, a bias is applied at the back surface of a silicon wafer, which acts as the anode, while a platinum mesh acts as the cathode, both of which are immersed in hydrogen fluoride (HF) electrolyte. Electrical holes drift towards the interface of the silicon and the electrolyte, where porous silicon forms [10]. A 3D silicon micromachining process using high energy ion beam irradiation and subsequent electrochemical etching of p-type bulk silicon wafers has been reported by our group [11–14]. This technique uses either the whole defect regions at high fluence to completely inhibit the etching process or localized defects created at the end of range of high-energy protons at a moderate fluence for fabrication of silicon structures within the bulk at certain depths, based on selective formation of porous silicon during subsequent anodization. A finely focused, high energy ion beam [11] is scanned over the silicon wafer surface. As the ion beam penetrates the semiconductor, the crystal lattice is damaged, producing additional defects which reduce the hole density and hole current [12]. The defect density for light ions, with energies greater than about 50 keV, peaks close to the end of their range [15]. By pausing the focused beam of different energies for different amounts of time at different locations, any pattern of localized damage can be built up. The irradiated wafer is then electrochemically anodized in an electrolyte of HF. At a high ion fluence, the irradiated regions completely inhibit the formation of porous silicon and remain as crystalline silicon, based on which Teo et al. reported the fabrication of a periodic array of sub-micron-diameter pillars [13], which is potentially important for the fabrication of photonic crystals. At a moderate ion fluence, only the buried regions with high defect density inhibit the porous silicon formation process. Thus, as the sample is etched beyond the depth of the ion range, the structure starts to become undercut due to isotropic etching, producing a silicon core that is surrounded by porous silicon. Multiple-energy proton irradiation can be used to create localized defects at different depths within the silicon wafer to fabricate multilevel 3D structures [14]. By varying the proton energy, the penetration depth changes, and subsequent etch steps enable fabrication of true 3D silicon free-standing structures [14]. We have previously reported 2D silicon-based photonic crystals with high flexibility, which shows the presence of a TE or TM gap in the mid-infrared range [16]. Tuning the band gap over a large range by changing the line period, line fluence, and etch current density was also reported [17]. Recently, defect-enhanced diffusion current in ion-irradiated regions, and how it induces porous silicon with high porosity and buried channels in porous silicon form, were reported [18, 19]. Here we present strategies, progress, and existing problems in fabrication and characterization of photonic crystals in the mid-infrared range using this method. The previous work in Refs. [16, 17] mainly discussed fabrication of 2D photonic crystals made of silicon, while here a much more general study is presented on the fabrication of mid-infrared photonic crystals with different dimensionalities made of both silicon and porous silicon. The current challenges faced in both fabrication and characterization of such structures are discussed. The advantage towards building integrated photonic circuits is demonstrated by the initial result on two 2D silicon photonic crystals on top of each other.

2 Experimental method

High-energy protons with energies of 100 keV to 1 MeV are focused down to a spot size of ∼100 nm, and used to create arbitrary 3D defect distributions by controlling the fluence on the surface of a p-type silicon wafer. The proton-irradiated wafer is subsequently electrochemically anodized in a 24 % HF electrolyte, which is prepared with 48 % HF:ethanol = 1:1, after which two different procedures are taken to form the structures. In one procedure, porous silicon is either removed by a simple dipping in dilute potassium hydroxide solution or left as the dielectric material in the resultant photonic crystals. In the other procedure, the samples are left in air for several weeks and dipped into dilute hydrogen fluoride electrolyte to remove the oxidized porous silicon.

3 Effect of fluence on the electrochemical anodization of p-type silicon

The ion fluence plays a major role in the formation of porous silicon and the resultant structures. Figure 1 shows the effect of proton fluence on the subsequent electrochemical anodization process and formation of hollow air wires surrounded by porous silicon at low fluence, formation of hollow air walls in porous silicon, and silicon wires in porous silicon at moderate fluence, as well as formation of silicon walls at high fluence. The left-most image in Fig. 1a shows the defect density distribution of 250 keV protons in silicon, which includes a low-defect region and a high-defect region

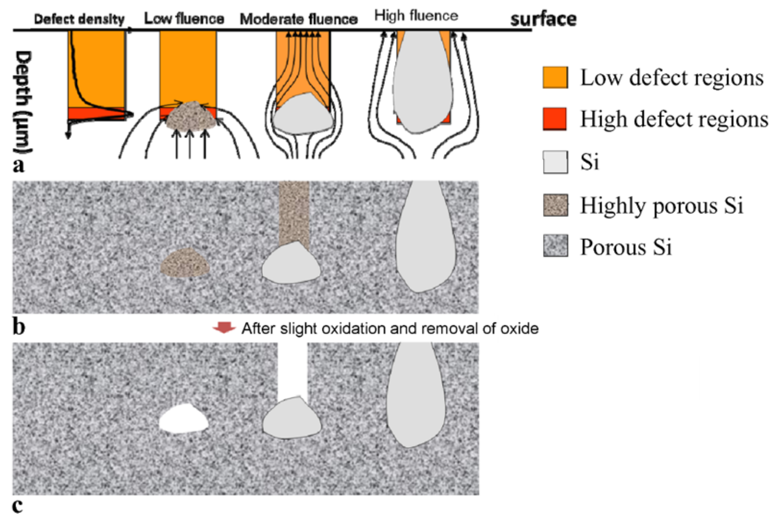

Fig. 1 (**a**) Left-most image shows the defect density distribution of 250 keV protons in silicon. Two different colors show two regions with obvious differences in the defect densities after irradiation. The three images to the right show hole current flow for three regimes of increasing proton fluence during electrochemical anodization; (**b**) formation of porous silicon in these three cases; (**c**) after mild oxidation and removal of oxide

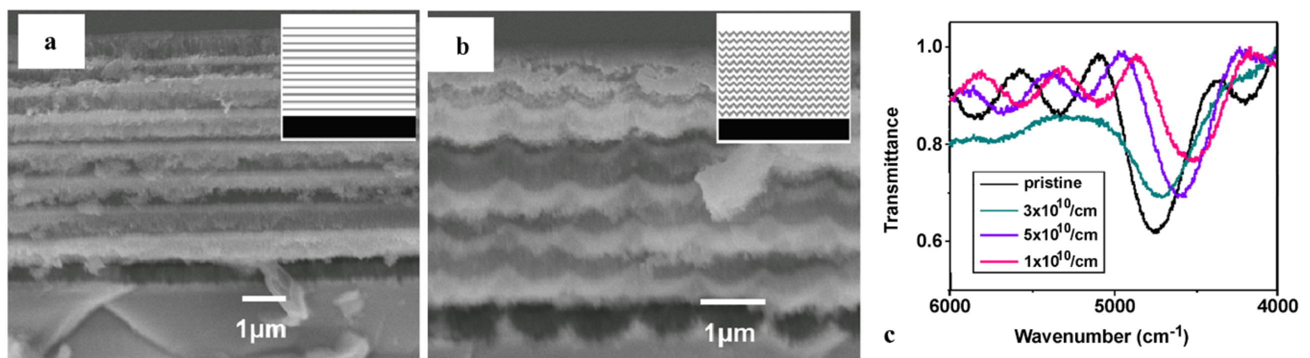

Fig. 2 (**a**) Cross-sectional SEM image of a porous silicon multilayer (*inset* shows the dielectric-constant function); (**b**) cross-sectional SEM image of modulated porous silicon multilayer irradiated by 1 MeV proton beam with 1 μm spacing, line fluence of 1×10^{11}/cm (*inset* shows the dielectric-constant function); (**c**) transmission spectra of structures in (**a**) and (**b**) modulated by three different line fluences

where the defect density is 10 times higher, identified by light and dark orange colors, respectively. The three right-hand images show three different regimes of proton fluence which result in different structures after anodization, where the difference of defect density caused by proton fluence is ignored and the same colors were used. Defects decrease the effective doping and hole density, which been discussed in previous work [12, 18, 19]: under low fluence, the diffusion current becomes dominant, leading to focused currents towards high-defect regions, which is shown in the second left figure of Fig. 1a. At moderate fluence, the potential from the high-defect region is high enough to deflect the total current away from the high-defect region, which, instead, is focused to the low-defect region [18, 19]. At high fluence, the potentials from both the low- and high-defect regions are high enough to deflect the total current away from the ion-irradiated regions. The resulting structure for the whole range of ion fluence is a buried porous silicon region with higher porosity for low fluence, a silicon wire buried in porous silicon in addition to a highly porous silicon column above the silicon wire for moderate fluence, and a silicon wall standing in porous silicon for high fluence, as shown in Fig. 1b. Porous silicon with higher porosity is oxidized in air easily and, after removal of the oxide, a hollow air wire surrounded by porous silicon forms for low fluence, while a hollow trench between porous silicon walls forms for moderate fluence, as shown in Fig. 1c.

3.1 Modulation of porous silicon based 1D photonic crystal (Bragg reflector)

Porous silicon based Bragg reflectors have been widely studied. The effect of ion-beam irradiation to reduce the etching rate and cause a blue shift of the response was also studied in previous work [20]. In this work, 1 MeV protons (focused to 100 nm) are used to modify the Bragg reflector profile, with the aim of fabricating a 2D photonic crystal based on a modified Bragg reflector by inducing a periodicity in the direction parallel to the surface. Fourier transform infrared (FTIR) spectroscopy was used to measure the transmission spectra. Figure 2a shows a cross-sectional scanning

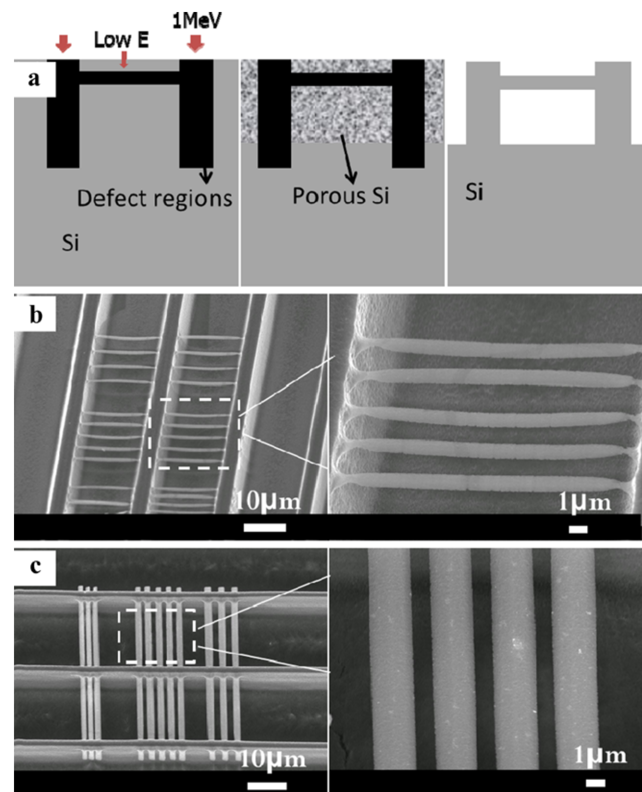

Fig. 3 Free-standing silicon wires. (**a**) Schematics of free-standing silicon wire formation: proton beam writing and resultant defect distribution in silicon (*left-most figure*), formation of porous silicon during subsequent etching (*middle figure*), removal of porous silicon (*right-most figure*); (**b**) using 250 keV proton line fluence of 1×10^{11}/cm; (**c**) using 218 keV proton line fluence of 1×10^{11}/cm, supported by walls irradiated by 1 MeV protons with high fluence

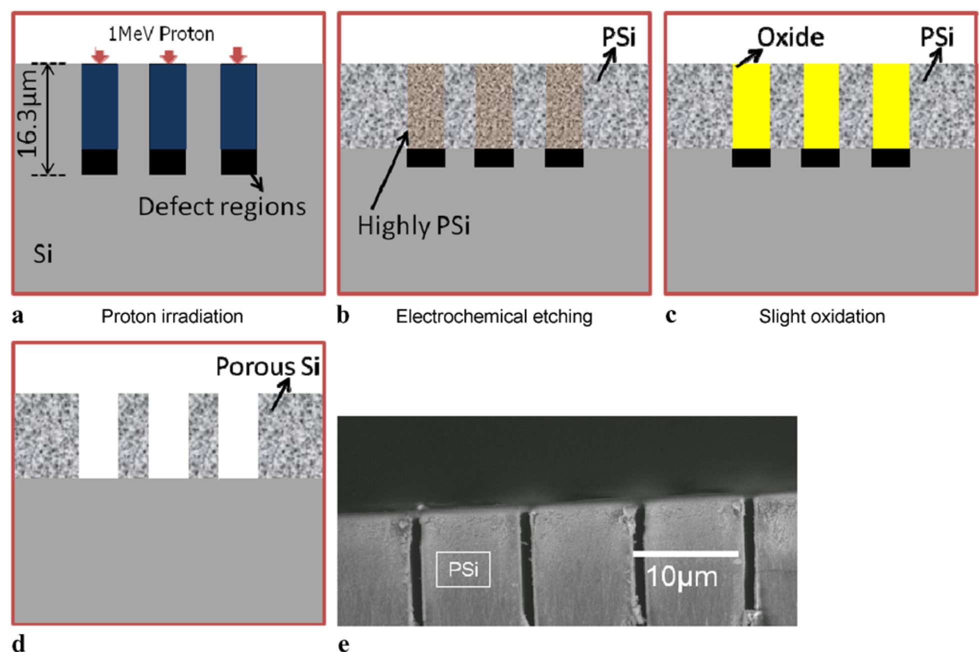

Fig. 4 Moderate fluence: (**a**) proton beam writing and induced defect regions; (**b**) formation of porous silicon during electrochemical etching process; (**c**) oxidation of highly porous silicon regions in air; (**d**) removing the oxidized regions to produce air trenches in porous silicon matrix; (**e**) cross-sectional SEM image of trenches in porous silicon

electron microscope (SEM) image of a porous silicon multilayer where a 0.02 Ω cm p-type silicon wafer was etched at an alternating current density of 50 mA/cm^2 for 15 s and 85 mA/cm^2 for 15 s in 12 % HF (48 % HF:ethanol:DI water = 1:2:1). Figure 2b shows a cross-sectional SEM image of a modulated porous silicon multilayer where the wafer was irradiated with a 100 nm wide 1 MeV proton beam to a line fluence of 1×10^{11}/cm, with a spacing of 1 μm, before etching, while the etching conditions are the same as in Fig. 2a.

By varying the line fluence, the curvature of the modulated profile is changed. The higher the line fluence, the larger the curvature, and hence a greater modulation of the transmission spectrum. However, proper design of the irradiation period, layer thickness, and porosity is needed for

achieving a 2D photonic crystal. Figure 2c shows the transmission spectra of the modulated porous silicon multilayers with three different line fluences, compared to the pristine multilayer, which was measured with incident angle of 0° in FTIR. The right shift of the dip is due to a reduction in etching rate, and the dip becomes shallower as the line fluence increases.

3.2 Fabrication of silicon-based 1D photonic crystal (grating)

In Ref. [16], the fabrication of free-standing silicon wires was discussed which could be regarded as a 1D photonic crystal equivalent to 1D gratings. Figure 3a shows a schematic of how free-standing silicon wires are fabricated. Figure 3b shows wires fabricated by 250 keV protons focused to 100 nm, with a line fluence of 1×10^{11}/cm, in 0.02 Ω cm p-type silicon. Figure 3c similarly shows wires fabricated using 218 keV protons which were focused to 100 nm with a line fluence of 1×10^{11}/cm, in 0.02 Ω cm p-type silicon, but here they are supported by walls irradiated by 1 MeV protons with high fluence. The figures to the right are magnified images of the regions within the white boxes. The spacing of each set of lines in (b) and (c) is 2, 3, and 4 μm.

3.3 Fabrication of porous silicon based 2D photonic crystal

Fabrication of silicon pillars and air hole slabs in a silicon matrix was discussed in detail in Refs. [16, 17], for which air and silicon are the two dielectric materials giving rise to dielectric-constant contrast. Here fabrication of 2D photonic crystals made of porous silicon where air and porous silicon are the two dielectric materials giving rise to a band gap is proposed based on a study of the etching mechanism due to low and moderate fluences in Refs. [18, 19]. In Fig. 4a, 1 MeV protons are used to irradiate at a moderate fluence. The dark blue color demonstrates the low defect density region where high-porosity silicon forms, while the dark color demonstrates the high defect density region where current is deflected away so this region remains as silicon. In the etching process, porous silicon with higher porosity forms in the low defect density region as shown in Fig. 4b, surrounded by porous silicon. The higher-porosity silicon is easily oxidized in air as shown in Fig. 4c; by removing it trenches or holes in a porous silicon matrix are obtained, as shown in Fig. 4d. Figure 4e shows a cross-sectional SEM image fabricated with 1 MeV protons with 1 μm line width on the surface, and a line fluence of 4×10^{11}/cm, with a spacing of 10 μm, in 0.02 Ω cm wafers.

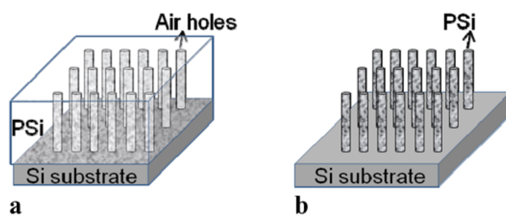

Fig. 5 (**a**) Air holes in porous silicon matrix on silicon substrate; (**b**) porous silicon pillars on silicon substrate

Two-dimensional porous silicon based photonic crystals with air holes in a porous silicon matrix in the mid-infrared range can be obtained by point irradiation and shrinking the spacing between the holes down to the size needed for the mid-infrared range, as shown in Fig. 5a. Such air hole structures in a porous silicon matrix have a greater height than air hole slabs in a silicon matrix which has a limited slab thickness [16, 17]; thus, we can solve the problem faced in characterization using FTIR spectroscopy. Similarly, by irradiation of intersecting lines as in the fabrication of air hole slabs in a silicon matrix [16], circular-shape porous silicon regions form at moderate fluences, as shown in Fig. 5b.

3.4 Towards 3D woodpile structure

In Ref. [16], the fabrication of a 3D woodpile structure was proposed. However, accurate alignment is difficult for different level structures due to ion-beam drift and stage-positioning inaccuracy. To solve the alignment problem, an

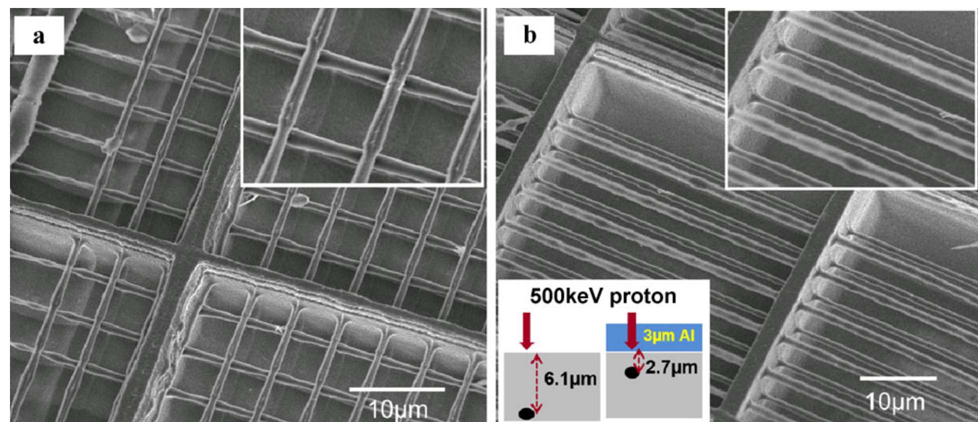

Fig. 6 (**a**) Bi-layer silicon wires fabricated by 500 keV and 400 keV protons, with ranges in silicon of 6.1 μm and 4.5 μm; (**b**) a bi-layer of silicon wires fabricated using 500 keV protons, without and with a 3 μm thick aluminum membrane, resulting in ranges of 6.1 μm and 2.7 μm (as shown in *inset* schematics), with line fluence of 3×10^{10}/cm

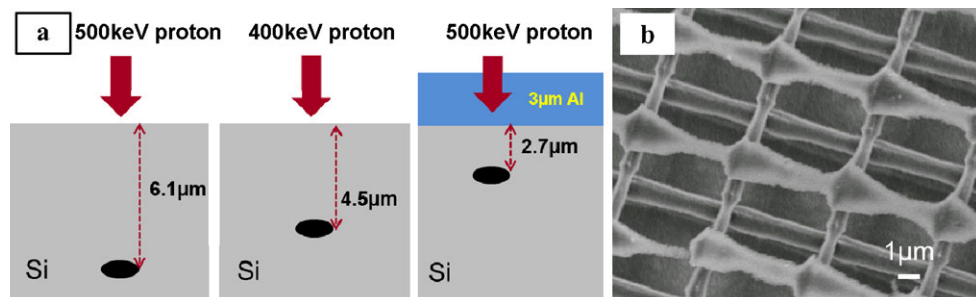

Fig. 7 (**a**) Schematics of generation of high defect regions at three different depths; (**b**) Tri-layer silicon wires fabricated by 500 keV, 400 keV, and 500 keV protons after passing through 3 μm aluminum membrane, giving ranges of 6.1, 4.5, and 2.7 μm in Si respectively

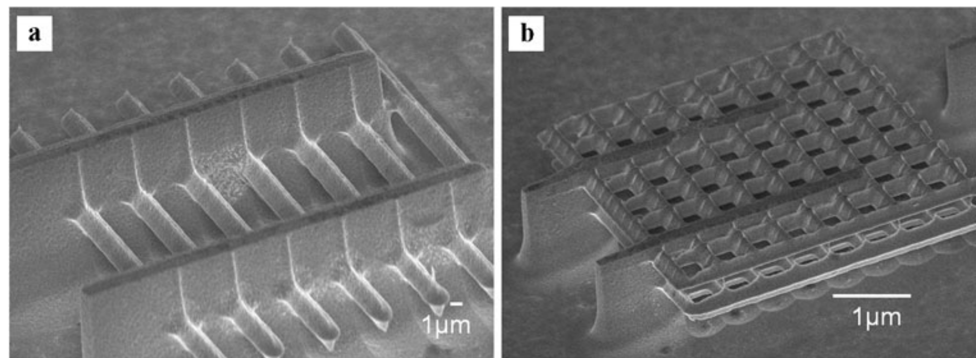

Fig. 8 (**a**) Free-standing silicon wires at 6.95 μm depth; (**b**) two levels of photonic crystal slabs at 7.0 μm and 2.4 μm depths

aluminum membrane was translated across the silicon wafer surface to reduce the ion-beam energy without changing the terminal voltage of the accelerator. In Fig. 6a bi-layer array of silicon wires fabricated using 500 keV and 400 keV protons is shown. Their ranges in silicon are 6.1 μm and 4.5 μm, respectively. A line fluence of 3×10^{10}/cm and a spacing of 5 μm were used with lines in a perpendicular direction. In Fig. 6b, a bi-layer of silicon wires was fabricated by a single incident proton beam energy of 500 keV, with the range in silicon changed by a 3 μm thick aluminum membrane from 6.1 μm to 2.7 μm.

By a combination of these three energies, tri-layer silicon wires have been fabricated, as shown in Fig. 7.

The uppermost layer of silicon wires shows inadequate ion fluence, due to the scattering of the focused ion beam after passing through the gap between foil and silicon surface. Therefore, a compromise between the chance of breaking the foils and a small gap needs to be made.

3.5 Towards compact photonic circuit

One of the main advantages of using proton beam writing combined with the electrochemical etching method for photonic crystals is the ability to allow separate structuring at different depths, for moving towards a compact photonic circuit. Figure 8b shows two 2D photonic crystals at depths of 7.0 μm and 2.4 μm, which were fabricated by using a proton beam with 550 eV and 250 keV, respectively, in a0.02 Ω cm wafer. Figure 8a shows wires at 6.95 μm depth in one direction.

4 Conclusion

Fabrication of 1D and 2D photonic crystals in the mid-infrared range, based on silicon and porous silicon, has been demonstrated, in addition to silicon-based pillars and air hole slabs shown in previous work. The possibility of a 3D woodpile structure in the mid infrared was discussed further by showing the recent advances in the fabrication approach. Combining proton beam writing with electrochemical etching of p-type silicon is a very promising approach towards silicon and porous silicon based mid-infrared photonic crystals and silicon-based photonic circuits.

References

1. E. Yablonovitch, Phys. Rev. Lett. **58**, 2059 (1987)
2. T.F. Krauss, R.M.D.L. Rue, S. Brand, Nature **383**, 699 (1996)
3. M. Notomi, A. Shinya, S. Mitsugi, E. Kuramochi, H.-Y. Ryu, Opt. Express **12**, 1551 (2004)
4. C. Monat, P. Domachuk, B.J. Eggleton, Nat. Photonics **1**, 106 (2007)
5. J.-H. Park, L. Gu, G. von Maltzahn, E. Ruoslahti, S.N. Bhatia, M.J. Sailor, Nat. Mater. **8**, 331 (2009)
6. S.W. Leonard, J.P. Mondia, H.M. van Driel, O. Toader, S. John, K. Busch, A. Birner, U. Gösele, V. Lehmann, Phys. Rev. B **61**, R2389 (2000)
7. W.-Y. Chiu, T.-W. Huang, Y.-H. Wu, Y.-J. Chan, C.-H. Hou, H.T. Chien, C.-C. Chen, Opt. Express **15**, 23 (2007)
8. M. Hermatschweiler, A. Ledermann, G.A. Ozin, M. Wegener, G. von Freyman, Adv. Funct. Mater. **17**, 2273 (2007)

9. S. Matthias, F. Müller, U. Gösele, Proc. SPIE **6182**, 12 (2005)
10. V. Lehmann, *Electrochemistry of Silicon: Instrumentation, Science, Materials and Applications* (Wiley-VCH, New York, 2002)
11. M.B.H. Breese, D.N. Jamieson, P.J.C. King, *Materials Analysis Using a Nuclear Microprobe* (Wiley, Chichester, 1996)
12. M.B.H. Breese, F. Champeaux, E.J. Teo, A.A. Bettiol, D.J. Blackwood, Phys. Rev. B **73**, 035428 (2006)
13. E.J. Teo, M.B.H. Breese, E. Tavernier, A.A. Bettiol, F. Watt, M. Liu, D.J. Blackwood, Appl. Phys. Lett. **84**, 3202 (2004)
14. S. Azimi, M.B.H. Breese, Z.Y. Dang, Y. Yan, Y.S. Ow, A.A. Bettiol, J. Micromech. Microeng. **22**, 015015 (2012)
15. J.F. Ziegler, M. Ziegler, J. Biersack, Nucl. Instrum. Methods Phys. Res., Sect. B, Beam Interact. Mater. Atoms **268**, 1818 (2010)
16. Z.Y. Dang, M.B.H. Breese, G. Recio-Sánchez, S. Azimi, J. Song, H.D. Liang, A. Banas, V. Torres-Costa, R.J. Martín-Palma, Nanoscale Res. Lett. **7**, 416 (2012)
17. G. Recio-Sánchez, Z.Y. Dang, V. Torres-Costa, M.B.H. Breese, R.J. Martín-Palma, Nanoscale Res. Lett. **7**, 449 (2012)
18. S. Azimi, Z.Y. Dang, J. Song, M.B.H. Breese, E. Vittone, J. Forneris, Appl. Phys. Lett. **102**, 042102 (2013)
19. Z.Y. Dang, J. Song, S. Azimi, M.B.H. Breese, J. Forneris, E. Vittone, Nucl. Instrum. Methods Phys. Res., Sect. B, Beam Interact. Mater. Atoms **296**, 32 (2013)
20. M.B.H. Breese, D. Mangaiyarkarasi, Opt. Express **15**, 9 (2007)